Communication

Rotation-facilitated rapid transport of nanorods in mucosal tissues

Miaorong Yu, Jiuling Wang, Yiwei Yang, Chunliu Zhu, Qian Su, Shiyan Guo, Jiashu Sun, Yong Gan, Xinghua Shi, and Huajian Gao

Nano Lett., **Just Accepted Manuscript** • DOI: 10.1021/acs.nanolett.6b03515 • Publication Date (Web): 04 Oct 2016

Rotation-facilitated rapid transport of nanorods in mucosal tissues

Miaorong Yu[1,4]#, Jiuling Wang[2,3,4]#, Yiwei Yang[1,4]#,Chunliu Zhu[1], Qian Su[2,3,4], Shiyan Guo[1], Jiashu Sun[2,4], Yong Gan[1,4], Xinghua Shi[2,3,4]*, Huajian Gao[5]**

[1]Shanghai Institute of Materia Medica, Chinese Academy of Sciences, Shanghai 201203

[2]CAS Key Laboratory for Nanosystem and Hierarchy Fabrication, CAS Center for Excellence in Nanoscience, National Center for Nanoscience and Technology, Chinese Academy of Sciences, Beijing 100190

[3]LNM, Institute of Mechanics, Chinese Academy of Sciences, Beijing 100190

[4]University of Chinese Academy of Sciences, NO.19A Yuquan Road, Beijing 100049

[5]School of Engineering, Brown University, Providence, RI 02912, USA

Corresponding authors: ygan@simm.ac.cn (Y. Gan), shixh@nanoctr.cn (X. Shi), huajian_Gao@brown.edu (H. Gao)

#These authors contributed equally to this work.

ABSTRACT

Mucus is a viscoelastic gel layer that typically protects exposed surfaces of the gastrointestinal (GI) tract, lung airways, and other mucosal tissues. Particles targeted to these tissues can be efficiently trapped and removed by mucus, thereby limiting the effectiveness of such drug delivery systems. In this study, we experimentally and theoretically demonstrated that cylindrical nanoparticles (NPs), such as mesoporous silica nanorods and calcium phosphate nanorods, have superior transport and trafficking capability in mucus compared with spheres of the same chemistry. The higher diffusivity of nanorods leads to deeper mucus penetration and a longer retention time in the GI tract than that of their spherical counterparts. Molecular simulations and stimulated emission of depletion (STED) microscopy revealed that this anomalous phenomenon can be attributed to the rotational dynamics of the NPs facilitated by the mucin fibers and the shear flow. These findings shed new light on the shape design of NP-based drug delivery systems targeted to mucosal and tumor sites that possess a fibrous structure/porous medium.

KEYWORDS: mucus penetration, nanoparticle diffusion, shape dependent, molecular simulations, transmucosal delivery.

Improving the mucus-penetrating ability of nanoparticles (NPs) is of great importance to avoid rapid drug clearance and achieve efficient drug delivery[1-3]. Mucus is a tenacious mesh structure with a thickness ranging from tens to hundreds of microns and an average pore size in the range of hundreds of nanometers[4]. Small hydrophilic molecules can freely diffuse through this barrier while particles, especially foreign particles, are excluded in cases where the particle size is larger than the average pore size[5-9]. The trapped particles are then quickly washed away by the microflows of the mucus layer. Such a capture and clearance mechanism protects mucosal tissues against infectious agents; however, this mechanism limits opportunities for the controlled drug delivery of NPs.

Innovative designs regarding the physicochemical properties of NPs are continuously arising to overcome this mechanical and physiological barrier[10-16]. According to the Stokes-Einstein equation, decreasing the NP size leads to an increase in the diffusion coefficient, making it easier for smaller particles to penetrate through the mucus[13]. However, small NPs with high surface areas exhibit burst effects, which lead to poor efficacy at the targeted tissues[17]. Moreover, extremely small NPs (2-10 nm) would yield inefficient cellular uptake[18, 19]. Surface charge can also influence the mucus-penetrating property, and neutral NPs have been suggested to effectively penetrate through the negatively charged intestinal mucus[14]. Inspired by the viruses that are capable of diffusing in mucus as fast as in water[5], Hanes *et al*[15, 16] designed high-density NPs free of surface charge by coating particles with low-molecular-weight poly(ethylene glycol) (PEG). They found that the PEGylation of NPs could improve the transport of these NPs through the mucus barrier. In addition to these studies that focused on the surface chemistry of NPs, it has also been recognized that shape may affect the diffusion of particles in porous media[20-22] and cellular uptake of NPs[23-27]. For example, Geng et al. demonstrated that filomicelles have much

longer circulation time than spherical counterparts[28]. Barua et al. have studied specific and nonspecific uptake of spherical, rod- and disk-shaped polystyrene NPs, and shown rods exhibited higher specific uptake and lower nonspecific uptake in three breast cancer cell lines[29]. Actually, most of the bacteria possessing a high mobility in mucus have a rod-like shape[30, 31]. Pathogens such as Helicobacter pylori[32] and Vibrio cholera[33] are able to swim through the intestinal mucus and remain in the mucus layer for extended periods, instead of being easily washed away. This finding informs us that shape may contribute to the high mucus-penetrating ability of particles. The correlation between the shape of NPs and their diffusivity in mucus, however, is still missing, even though this aspect is potentially crucial in the design of NPs-based drug delivery systems.

We hypothesized that engineered nanorods may penetrate the mucus layer more efficiently than nanospheres. To verify this hypothesis, we fabricated mesoporous silica nanospheres (MSNSs) and mesoporous silica nanorods (MSNRs) with different aspect ratios (ARs) but identical surface chemistries and zeta potentials. We present evidence that, compared with spheres, cylindrical NPs display superior diffusion and penetration patterns in intestinal mucus, which can further lead to a longer intestinal retention time and higher villus absorption. Molecular simulations and stimulated emission of depletion (STED) microscopy revealed that the rotational diffusion of nanorods within the complex mucus structure plays an active role in such diffusion enhancement.

To elucidate the effect of shape on the mucus-penetrating property of NPs, highly mono-dispersed MSNSs (MSNS1 and MSNS2) and MSNRs with identical surface charges and chemical compositions but with different ARs were fabricated following previously reported procedures[34, 35]. The morphology of the NPs was revealed in transmission electron microscopy

(TEM) images (Fig. 1a) in which the MSNS1 has a diameter of approximately 80 nm (AR=1), MSNS2 has a diameter of approximately 140 nm (AR=1), and the MSNRs have a dimension of approximately 80×240 nm (AR=3). The hydrodynamic diameters of the MSNs were about 100 nm, 200 nm and 200 nm for MSNS1, MSNS2 and MSNRs, respectively (Fig. 1b). For *ex vivo* and *in vivo* tracking, the NPs were covalently labeled with rhodamine isothiocyanate (RITC) as previously reported[36]. The average zeta potentials of three types of labeled particles were approximately -5 mV (Fig. 1c), which has preference in penetrating the mucus mesh. The same zeta potential ensures the same electrical interaction patterns with mucins, thus keeping the shape as the only variable.

Multiple-particle tracking technology provides a non-destructive and highly sensitive method to determine particle behavior in complex biological environments[37]. We first used this method to investigate the movement of the NPs in fresh intestinal mucus. The trajectories of the particles were captured, and representative trajectories of MSNS1, MSNS2 and MSNRs were mapped in Fig. 1d. It was observed that MSNS1 and MSNS2 moved within a small area, indicating that these particles were nearly trapped by the mucus network. In contrast, the MSNRs were able to move more freely in a large area, displaying a better diffusion pattern. The accumulative mean square displacement (MSD) was calculated on a time scale of 1 s (Fig. 1e), and the MSD of the MSNRs was approximately 3.3-fold and 5.7-fold higher than that of MSNS1 and MSNS2, respectively (see Table S1). To ensure the observed rapid transport of MSNRs was not biased by a small fraction of fast-moving outlier particles, the distribution of effective diffusivities (D_{eff}) was examined. We confirmed that MSNRs persistently exhibit higher diffusivities compared to MSNSs (Fig. 1f). The distinct movement patterns suggest that MSNRs can penetrate the mucus more efficiently.

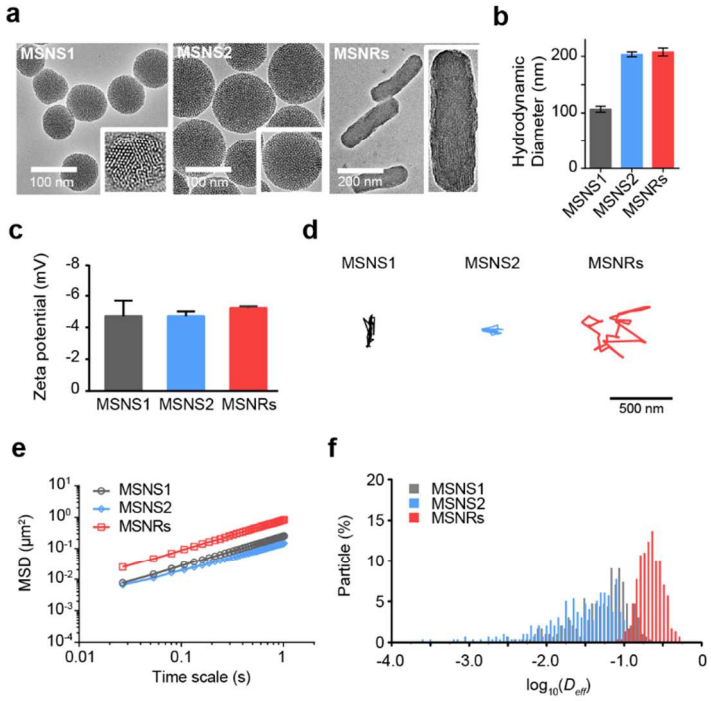

Figure 1. Characterization of the NPs and multiple-particle tracking studies. (**a**) TEM images of the MSNS1 (~80 nm), MSNS2 (~140 nm) and MSNRs (~80×240 nm). (**b**) Hydrodynamic diameter of the NPs according to dynamic light scattering tests. (**c**) Zeta potential of the NPs after RITC labeling. All the NPs had an average zeta potential of approximately -5 mV. (**d**) Representative trajectories for particles in the intestinal mucus on a time scale of 1s. (**e**) Ensemble-averaged geometric mean square displacement (MSD) as a function of time scale. (**f**) Distributions of the logarithms of individual particle effective diffusivities for MSNS1, MSNS2 and MSNRs at a time scale of 1 s. The data are presented as means ± standard error means (SEM) (n = 300).

We next focused on the rat intestinal loops to investigate whether a better mucus-penetrating ability would lead to a more uniform and deeper distribution of MSNRs compared with MSNS1 and MSNS2 *ex vivo*. To quantify the distribution patterns of the NPs, the mucin fibers were

stained with Alexa Fluor 488-conjugated wheat germ agglutinin (WGA), and particle solutions were injected into ligated intestinal loops, followed by a 30-min incubation with gentle agitation[38]. Fluorescence images of freshly excised, opened and flattened intestinal sections were obtained as depicted in Fig. 2a. Both MSNS1 and MSNS2 exhibited a low level of mucus coverage, whereas the MSNRs were widely dispersed in the mucus and had a uniform fluorescence intensity in the vast majority of the mucosal area. Quantification of the distribution area revealed that approximately 80% of the intestinal surface was covered with MSNRs, while MSNS1 and MSNS2 covered less than 15% (Fig. 2b). Further inspection of the mucus-penetration property via three-dimensional scanning (Fig. 2c) indicated that MSNS1 and MSNS2 could not effectively penetrate the mucus, and only a few particles were detected in the upper layer. In contrast, the MSNRs were transported deeper along the z-direction. Additionally, in order to eliminate potential heterogeneity of mucus, we performed co-injections of green and red fluorescent NPs of different shapes. Similar to the results observed above, MSNRs penetrated deeper into the intestinal mucus than MSNS1 and MSNS2 (Fig. 2d). As an appropriate control, the carboxylated fluorescent latex beads with diameter of 200 nm (red) were mixed with MSNs (green), and tested in the same mucus specimens (Supplementary Fig. 1). The MSNRs kept the superior penetrating ability as in other studies. It could be inferred that the poor diffusive capability of MSNS1 and MSNS2 led to their inferior penetration in the mucus, while the MSNRs effectively penetrated the mucus during the 30-min incubation period.

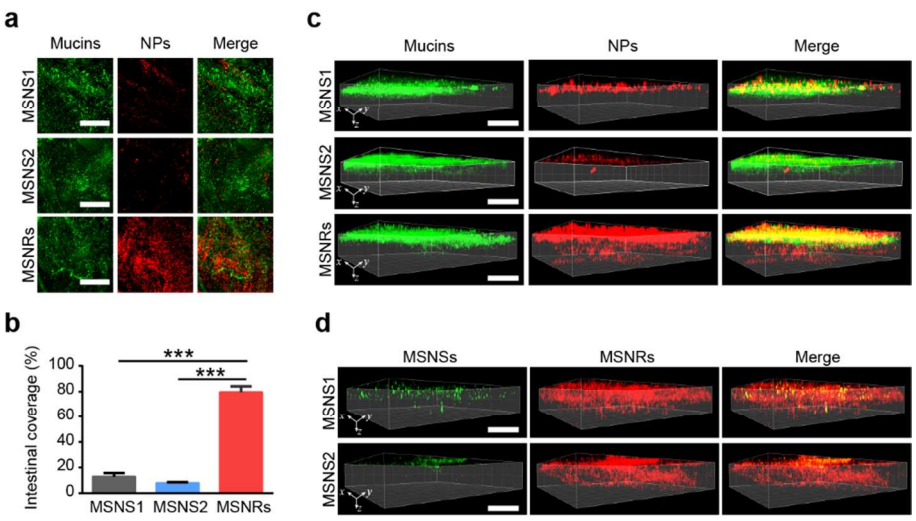

Figure 2. Particle distribution and penetration in the rat intestinal mucus *ex vivo*. (**a**) Two-dimensional coverage of NPs diffused in the intestinal mucus. (**b**) Quantification of the NP coverage in the mucus in (**a**). (**c**) Three-dimensional images of the mucus penetration. Green: mucus stained with Alexa Fluor 488-WGA. Red: NPs. (**d**) Direct comparison of penetration of MSNRs with MSNSs in the same mucus. Green: MSNS1 or MSNS2. Red: MSNRs. Images are representative of the averages. Scale bar: 50 μm. Depth: 40 μm. The data are presented as means ± standard error means (SEM) ($n \geq 3$). ***$P < 0.001$ compared to either MSNS1 or MSNS2.

To determine whether aggregation of the MSNSs hampered the mucus-penetrating process of the nanospheres, we decorated the NPs with a high density of PEG to further study the ability of these particles to penetrate mucus. The hydrodynamic diameters of the MSNS1-PEG, MSNS2-PEG and MSNRs-PEG were approximately 160 nm, 260 nm, and 285 nm, respectively. Particle tracking and distribution in mucus were investigated, and the results revealed that all three NPs had a significant enhancement of diffusivity in the mucus while the MSNRs-PEG kept the best mucus-penetration capability (Table S1, Supplementary Fig. 2). Since it has been reported that near-neutral potentials[14] and PEG modification could effectively reduce the interaction of

particles with mucus and enhance the particle stability, these results further demonstrated that the distinctive mucus-penetrating property resulted solely from the difference in shape.

We assessed whether better diffusion could contribute to more rapid and deeper intestinal penetration of MSNRs compared with MSNS1 and MSNS2 *in vivo*. Fasted SD rats were orally administered the fluorescently labeled NPs, and sections of the middle small intestine were collected and analyzed by confocal fluorescence microscopy (Fig. 3). There were few MSNS1 or MSNS2 at the lumenal side of GI tract and could not be discovered near the epithelial cells. In contrast, the MSNRs uniformly distributed along the surface of the intestinal villi with a strong intensity, which indicated that the penetration and absorption of the MSNRs were indeed more efficient than those of MSNS1 and MSNS2. A single intestinal villus was then carefully examined at a higher magnification. The MSNRs uniformly remained in close proximity to the intestinal epithelium and efficiently entered the intestinal tissue, while very few MSNS1 or MSNS2 appeared in the regions of interest. We note that the microscopy data provides evidence of superior absorption of the rods when compared to the spheres - however the absolute extent of absorption is difficult to evaluate via microscopy. To further ensure the difference between MSNRs and MSNSs, different fluorophores labeled particles were co-administrated, and the results showed that MSNRs maintained the superiority in mucus-penetration (Supplementary Fig. 3). These *in vivo* studies confirmed that the distinct shape plays an active role in the bio-behavior of NPs within the mucus mesh and will determine the fate of NPs in biological systems.

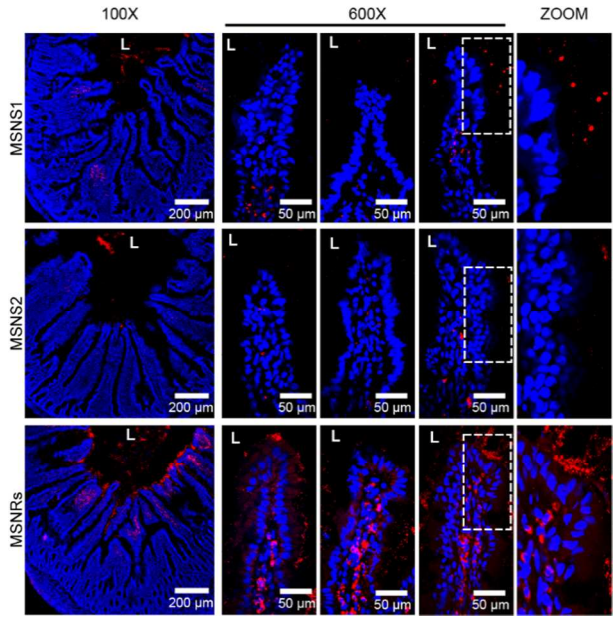

Figure 3. Particle distribution in the rat intestine. Particles gathering around or absorbed by the intestinal villi were carefully examined via confocal laser scanning microscopy (CLSM). Blue: nuclei of the intestinal villi. Red: NPs. L represents the intestinal lumen. Images were acquired 2 h after oral gavage.

Based on the results and conclusions mentioned above, it can be reasonably inferred that MSNRs can remain longer in the intestine, instead of being quickly washed out by the turnover of mucus. After intragastric administration, the entire stomach and small intestine were excised and imaged with an *in vivo* imaging system at specified time points (Fig. 4a). After a similar initial increase in fluorescence, the amount of MSNS1 and MSNS2 decreased quickly after 2 h, and little fluorescence could be detected after 6 h (Fig. 4b). In contrast, a considerable amount (approximately 40%) of the MSNRs remained in the jejunum and ileum even 6 h later. Since the fluorophore and particles remained stable in simulated gastric fluid (SGF) and simulated intestinal fluid (SIF) after 6 h (Supplementary Figs. 4 and 5), thus these images vividly revealed

that MSNRs had a better intestinal dispersion property and were more difficult to be washed away by the mucus, which could be attributed to the efficient mucus-penetrating property. Such a prolonged retention time should be beneficial to sustained drug release and absorption.

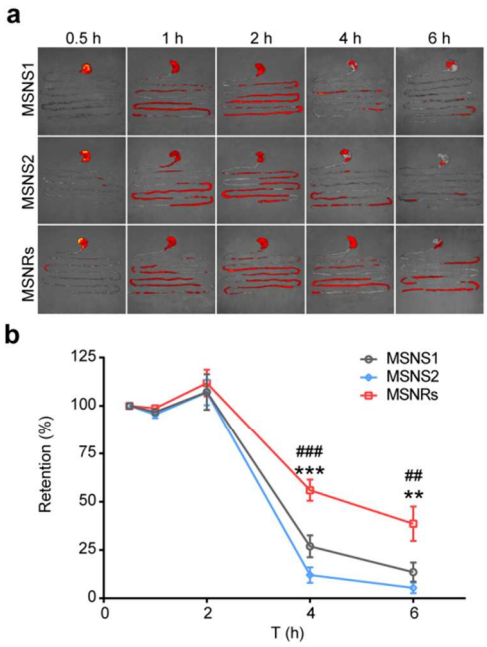

Figure 4. Particle retention in the rat GI tract. (**a**) Photographic images of NPs in tissues of th e whole small intestine. The images are representative of the average at each time point after intr agastric administration. (**b**) Fraction of particles remaining over time on the basis of quantificatio n of particle fluorescence. The data are presented as means ± standard error means (SEM) (n ≥ 3). $^{**}P < 0.01$ and $^{***}P < 0.001$ compared to MSNS1, $^{\#\#}P < 0.01$ and $^{\#\#\#}P < 0.001$ compared to MSNS2.

We additionally investigated whether the improved penetration of MSNRs could lead to superior drug delivery. The limited permeability of drug delivery particles and many hydrophobic molecules through the mucus barrier leads to their rapid clearance and thus poor bioavailability.

We used camptothecin (CPT) which has poor solubility and low permeability as a model drug. CPT, CPT-MSNS1, CPT-MSNS2 and CPT-MSNRs were loaded into intestinal loops, and the permeation of CPT through mucus to the intestinal wall was calculated. As expected, after 2 h, the CPT-MSNRs group had a 2.3, 2.4 and 2.6 fold higher level of total transported CPT than the CPT-MSNS1, CPT-MSNS2 and control groups, respectively (Supplementary Fig. 6b). Furthermore, a three-dimensional dispersion view of CPT was captured (Supplementary Fig. 6a), and the results were in accordance with the particle distribution. We noted that these CPT-loaded particles were not significantly different regarding CPT release rate and quantity (Supplementary Fig. 6d); therefore, the superior mucus-penetrating ability of the CPT-MSNRs can enhance CPT transportation, and the nanorods can thus serve as an improved drug delivery system.

Mucus-penetrating capability is observed to be shape dependent, not only for mesoporous silica NPs, but also for the other material tested here, calcium phosphate NPs. We have investigated diffusion of calcium phosphate nanospheres (CaPSs) and calcium phosphate nanorods (CaPRs), with results confirming improved mucus-penetrating ability of CaPRs (Supplementary Fig. 7).

To elucidate the mechanisms for the unexpected superior mucus-penetrating ability of nanorods, we conducted coarse-grained (CG) molecular dynamics (MD) simulations to investigate the diffusion of the NPs in mucus. To simplify this problem, we constructed a model system composed of cross-linked polymers, water and NPs. A regular polymer network was utilized to represent mucus fibers with a mesh size of 6σ (σ is the unit of length). The size of the simulation box was $48\times54\times48\sigma$, and periodic boundary condition was applied in all three directions. In each simulation system there were 96,984 coarse-grained water beads, 208 polymers (the polymers consisted of 9,261 beads, and the content of the polymers was approximately 8.5%)

and 40 NPs. The NPs were randomly distributed in the system as shown in Fig. 5b. Three types of NPs, nanosphere with diameter of 3.5σ (NS3.5), nanorods with size of $2.1\times4.6\sigma$ (NR2.1*4.6) and $1.8\times5.8\sigma$ (NR1.8*5.8), were studied in our simulation (Fig. 5a). The sizes of these NPs were calibrated so that they had the same hydrodynamic diameter (Supplementary Fig. 9). The simulation was implemented with the LAMMPS package[39].

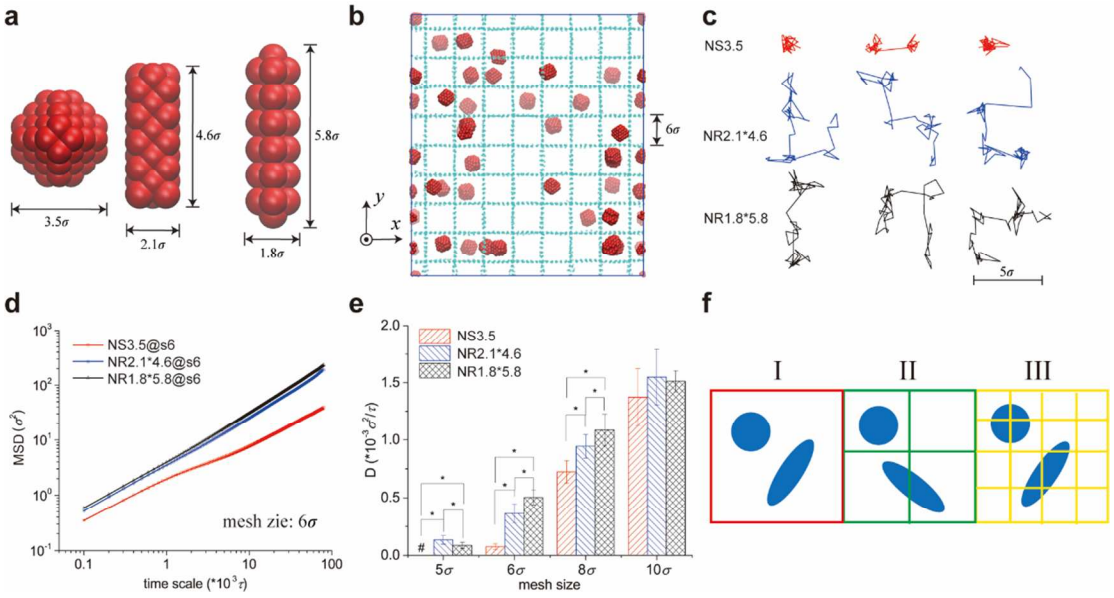

Figure 5. Snapshots and trajectories for the movement of NPs in mucin fibers. (**a**) The construction of three types of NPs. The NPs are created by a face-centered cubic (FCC) lattice with a Lennard-Jones reduced density of 8. **(b)** NPs and polymer network. The simulation system is composed of water, polymers (cyan) and NPs (red); for clarity, water molecules are not shown. Panel (**c**) shows translational centroid trajectories for one typical NP in one simulation. Panels (**d**) show the MSDs for NPs when the polymer network mesh size is 6σ. The red, blue and black dots represent nanospheres, nanorods with size of $2.1\times4.6\sigma$ and $1.8\times5.8\sigma$, respectively. Panel (**e**) lists all the calculated diffusivities of NPs in polymer networks with different mesh sizes. Error

bars are presented as standard error of the mean. The method to calculate the diffusivities is shown in the Methods. The symbol # indicates the diffusivity of NS3.5 is close to zero. (**f**) Schematic showing the diffusion of NPs in networks with different mesh sizes. I: free diffusion; II: obstructive diffusion; III: stagnant diffusion. (*$P < 0.05$)

Fig. 5b depicts typical snapshots of the diffusion of NPs in the polymer network. Fig. 5c indicates the translational trajectories for typical nanospheres and nanorods in one simulation. Notably, it is observed that the nanorods diffuse faster than the nanospheres. We repeated the simulation 8 times with different starting configurations and obtained the MSDs for NS3.5 (red dot), NR2.1*4.6 (blue dot) and NR1.8*5.8 (black dot) NPs as revealed in Fig. 5d. There is a distinct difference between the MSDs of the nanospheres and nanorods: the MSD of the nanorods is much higher than that of the nanospheres. The calculated diffusivity of NR2.1*4.6 is 4.94-fold that of NS3.5, and even higher for NR1.8*5.8 (6.28-fold that of NS3.5) (Fig. 5e). It seems the thin NPs could gain enhanced diffusivity in the polymer network. We also changed NPs-polymers interaction, polymers-water interaction, and NPs-water interaction to model variations in materials of NPs and polymers. All the results indicate that the nanorods have superior diffusivity in comparison to the nanospheres, suggesting the robustness of our conclusions (Supplementary Fig. 10).

To explain why nanorods move faster than nanospheres, we selected two representative NPs and analyzed their moving trajectories. Fig. 6 displays the translational displacement of one typical nanorod along the y direction (Δy) and the rotating angle around the z-axis (θ_z). It was observed that the translational movement of nanorod along the y direction is accompanied by rotation, especially when the NPs jump from one unit cell of a fiber network to another, as shown in Fig.

6c. For nanorods, it appears that, rotation around the polymer chain fundamentally contributes to the translational diffusion. The rotational dynamics of nanorods were also confirmed using STED microscopy (Fig. 6d and 6e, Supplementary movie 1). A single MSNR is rotating in the mucus, which is consistent with the results of the molecular simulation. In comparison, no significant correlation was found between translational diffusion and rotation for the nanospheres. To further verify this hypothesis of rotation-facilitated enhanced diffusion, we conducted additional simulations in which the rotation of nanorods was constrained. The results show that the diffusivity of nanorods is reduced by 74% (Supplementary Fig. 14). Therefore, we concluded that the movement of nanorods consists of two parts, rotation around the polymers and translational diffusion. With this mechanism elucidated, we could explain the observed anomalous phenomenon in the experiments and simulations that nanorods move faster than nanospheres.

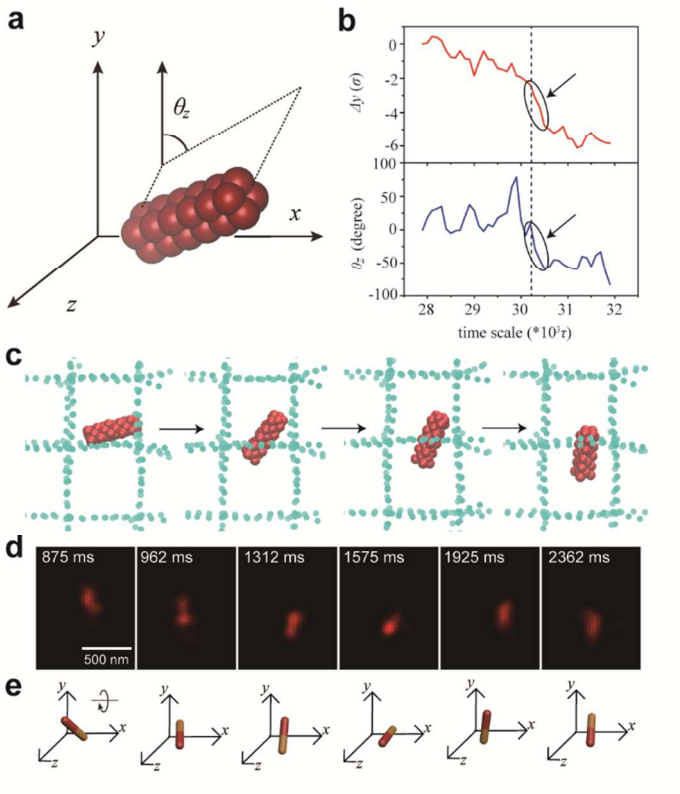

Figure 6. (**a**) Schematic of θ_z, the angle between the *y*-axis and the projection of the cylinder in an *xy* plane. (**b**) The displacement along the *y* direction and the rotational angle around the *z*-axis (θ_z) for one typical cylindrical NP. (**c**) A significant change in the position and orientation of cylindrical NPs at the moment the arrow points to in panel (**b**). (**d**) Snapshots and trajectories for an individual MSNR in mucus, as imaged with STED microscopy. The MSNRs have a rod-like shape with one end brighter than the opposite end. (**e**) Corresponding 3D schematic drawings of position and orientation of the MSNR in panel (**d**). The brighter end of the rod is colored red, and the opposite end is colored orange. The nanorod clearly rotates around a certain axis (Fig. 6**d** and **e** and Supplementary movie 1).

To further investigate which factors influence the diffusion of NPs, we first changed the mesh size of the polymer network to study the effect of pore size. When the mesh size is 5σ, the

diffusivity of NS3.5 is close to zero, whereas those of nanorods are finite (Fig. 5e). As the mesh size increases to 8σ, however, the advantage of diffusion for nanorods is not so evident anymore (Fig. 5e). When the mesh size reaches to 10σ, the diffusivity of NR2.1*4.6 and NR1.8*5.8 is only 1.1-fold and 1.12-fold that of NS3.5, approaching the cases in pure water (Fig. 5e). These findings suggest that the nanorods outperform nanospheres in diffusivity only in a range of mesh size around 6σ. Hanes *et al*. has shown that mucus pores are irregular in size and mucus with pore size no bigger than the particle size would create a "sieve" that sterically obstructs the diffusion of nanoparticles[2]. Based on this concept, there could be three types of diffusion regions in mucus: free diffusion, obstructive diffusion and stagnant diffusion, as shown in Fig. 5f. Those particles that have passed through the free diffusion region would eventually encounter their diffusion bottle neck in obstructive and stagnant regions. Enhancing the diffusivity of nanoparticles in these two regions thus becomes the key to increase the overall diffusivity. According to our simulation results, the advantage of nanorods in diffusivity is attributed to their enhanced diffusion in the obstructive and stagnant diffusion regions.

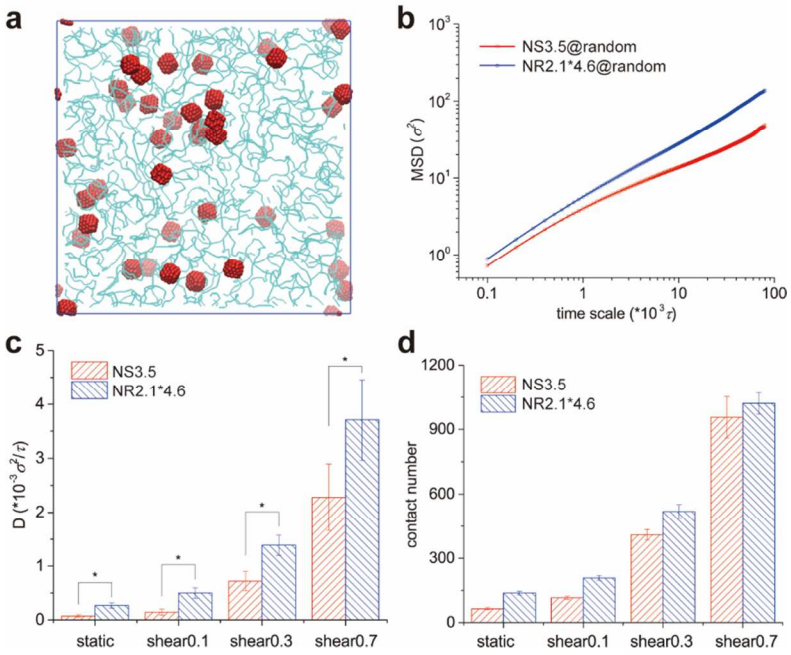

Figure 7. Diffusion of NPs in random network. (a) Schematic diagram of random polymer network used in the simulation, polymers are in cyan and NPs in red. **(b)** MSD of NPs in random polymer network. **(c)** Diffusivities of NPs in shear flow. shear0.1, shear0.3 and shear0.7 denote the coefficient $F_{\max}$ in drag force formula is 0.1, 0.3 and 0.7. **(d)** The number of NPs in contact with a background polymer network during a 10^4 τ simulation. (*$P < 0.05$)

Consider the heterogeneity of mucus pore sizes[40], we have also constructed a model system composed of cross-linked polymer network with random pore size (See Methods for details) to represent mucin fibers, as shown in Fig. 7a. In this model, the pore sizes distributed from 3σ to 10σ (Supplementary Fig. 13), similar to those observed in experiment (Supplementary Fig. 8). Nanorods in this heterogeneous fibrous media also exhibit significant enhanced diffusivity, as shown in Fig. 7b and Table S1.

We have also studied the diffusion of NPs in random polymer network under oscillatory shear flow, which mimics the movement of NPs during GI peristalsis and the disturbed environment in experiments. We applied shear flow by adding a drag force $F_{\text{add}} = F_{\max} y\varepsilon/\left(L_y\sigma\right)$ to each water bead, where y and L_y are the coordinates of atoms and the box size along the y direction, respectively, $F_{\max}$ is a coefficient and ε is the unit of energy. We reversed the force direction every 200,000 time steps, through which the oscillatory shear flow along the x direction was applied. The diffusivities of NPs are shown in Fig. 7c, where nanorods show higher diffusivity than nanospheres under all conditions. Meanwhile, the diffusivity of NPs increases with the shear rate. It implies that disturbed fluid environment contributes to the diffusion of NPs in mucus system. Note that we exclude the movement of NPs along the x direction during the calculation of the MSD because the oscillatory shear flow is applied along the x direction.

This shear-flow-enhanced diffusion could also be elucidated from the streamline around the NPs as revealed in Supplementary Fig. 15, in that the water flow could push one part of the cylindrical NP to rotate. This high diffusivity may be attributed to the high probability that NPs will encounter the polymer network in the shear flow, which facilitates the rotational motion of cylindrical NPs (Fig. 7d).

In summary, we have demonstrated that mesoporous silica nanorods can diffuse faster than nanospheres in mucus, which results in a longer intestinal retention time, higher penetration of drug or particle to the absorptive surface. Combining the experiments with the molecular simulations, we found that the better mucus-penetrating property of the nanorods is due to the rotational motions of the nanorods facilitated by the shear flow and the mesh structure of mucus. Additionally, to confirm that this property is not limited to a specific type of materials, we have fabricated calcium phosphate nanospheres (CaPSs) and calcium phosphate nanorods (CaPRs) and compared their diffusion and penetration behaviors in mucus, with results confirming that CaPRs exhibit better properties in *ex vivo* studies. Our work provides insights into the effect of NP shape on the mucus-penetrating property and demonstrates the usability of nanorods for drug delivery to mucosal tissues.

We note that in addition to transport in mucosal tissues, nanorods can have superiority in interstitial transport within the dense interstitial structure surrounding tumor cells[21]. Because the microenvironment of the interstitial structure is similar to that of mucus, which is formed by fibrous tissues, we postulate that the mechanism for the rapid penetration of nanorods into tumor sites may be the same as that for mucus. Therefore, although conventional spherical NPs currently remain the dominant shape, non-spherical NPs may become common next-generation

drug carriers[24, 28, 41, 42]. The barrier to using non-spherical particles lies partly with the difficulty in synthesis and characterization[43, 44] but even more with the lack of understanding of the physics that govern the relationship between shape and various characteristics of non-spherical NPs. Our findings may inspire the novel and rational design of drug delivery systems for use in various diseases.

ASSOCIATED CONTENT

Supporting Information. Including experimental procedures, additional experiments, results and expanded discussions. This material is available free of charge via the Internet at http://pubs.acs.org.

AUTHOR INFORMATION

Corresponding Author

*Xinghua Shi (shixh@nanoctr.cn). *Yong Gan (ygan@simm.ac.cn). *Huajian Gao (huajian_Gao@brown.edu).

Author Contributions

Y.G., X.S., M.Y., J.W., Y.Y., and H.G. planned and executed the experiments, analyzed the data and were involved in discussions of the data. Y.G., X.S., M.Y., J.W., Y.Y., and H.G. wrote the manuscript. Y.Y. prepared the NPs and performed the multi-particle tracking experiments. M.Y. designed and performed the mucus penetration experiments. J.W., Q.S. and J.S. performed and analyzed the molecular simulations. C.Z., Q.S. and S.G. contributed materials. All the authors critically reviewed and approved the manuscript.

Acknowledgment

We are grateful for the financial support from the National Natural Science Foundation of China (81373356 and 81573378 to Y.G., 11422215, 11272327 and 11672079 to X.S.), the "Science and technology innovation action plan for basic research" of Shanghai 2014 (14JC1493200 to Y.G.). This work was also partly supported by Institutes for Drug Discovery and Development, Chinese Academy of Sciences (NO. CASIMM0120153020 to Y.G.). The computation is mainly supported by the Supercomputing Center of Chinese Academy of Sciences (SCCAS).

Competing financial interests

The authors declare no competing financial interests.

REFERENCES

1. Lai, S. K.; Wang, Y. Y.; Hanes, J. *Adv. Drug Delivery Rev.* **2009,** 61, 158-71.
2. Ensign, L. M.; Cone, R.; Hanes, J. *Adv. Drug Delivery Rev.* **2012,** 64, 557-70.
3. Cu, Y.; Saltzman, W. M. *Nat. Mater.* **2009,** 8, 11-13.
4. Cone, R. A. *Adv. Drug Delivery Rev.* **2009,** 61, 75-85.
5. Olmsted, S. S.; Padgett, J. L.; Yudin, A. I.; Whaley, K. J.; Moench, T. R.; Cone, R. A. *Biophys. J.* **2001,** 81, 1930-7.
6. Horcajada, P.; Chalati, T.; Serre, C.; Gillet, B.; Sebrie, C.; Baati, T.; Eubank, J. F.; Heurtaux, D.; Clayette, P.; Kreuz, C.; Chang, J. S.; Hwang, Y. K.; Marsaud, V.; Bories, P. N.; Cynober, L.; Gil, S.; Ferey, G.; Couvreur, P.; Gref, R. *Nat. Mater.* **2010,** 9, 172-178.
7. Lieleg, O.; Ribbeck, K. *Trends Cell Biol.* **2011,** 21, 543-551.
8. Kirch, J.; Schneider, A.; Abou, B.; Hopf, A.; Schaefer, U. F.; Schneider, M.; Schall, C.; Wagner, C.; Lehr, C. M. *Proc. Natl. Acad. Sci. U. S. A.* **2012,** 109, 18355-18360.
9. Porter, C. J.; Trevaskis, N. L.; Charman, W. N. *Nat. Rev. Drug Discovery* **2007,** 6, 231-48.
10. Maisel, K.; Ensign, L.; Reddy, M.; Cone, R.; Hanes, J. *J. Controlled Release* **2015,** 197, 48-57.
11. Suk, J. S.; Kim, A. J.; Trehan, K.; Schneider, C. S.; Cebotaru, L.; Woodward, O. M.; Boylan, N. J.; Boyle, M. P.; Lai, S. K.; Guggino, W. B.; Hanes, J. *J. Controlled Release* **2014,** 178, 8-17.
12. Yu, T.; Chan, K. W.; Anonuevo, A.; Song, X.; Schuster, B. S.; Chattopadhyay, S.; Xu, Q.; Oskolkov, N.; Patel, H.; Ensign, L. M.; van Zjil, P. C.; McMahon, M. T.; Hanes, J. *Nanomedicine* **2015,** 11, 401-5.
13. Dawson, M.; Wirtz, D.; Hanes, J. *J. Biol. Chem.* **2003,** 278, 50393-401.

14. Laffleur, F.; Hintzen, F.; Shahnaz, G.; Rahmat, D.; Leithner, K.; Bernkop-Schnurch, A. *Nanomedicine (London, U. K.)* **2014,** 9, 387-96.
15. Lai, S. K.; O'Hanlon, D. E.; Harrold, S.; Man, S. T.; Wang, Y. Y.; Cone, R.; Hanes, J. *Proc. Natl. Acad. Sci. U. S. A.* **2007,** 104, 1482-7.
16. Wang, Y. Y.; Lai, S. K.; Suk, J. S.; Pace, A.; Cone, R.; Hanes, J. *Angew. Chem., Int. Ed. Engl.* **2008,** 47, 9726-9.
17. Fang, C.; Shi, B.; Pei, Y. Y. *Acta Pharmacol. Sin.* **2005,** 26, 242-249.
18. Gao, H. J.; Shi, W. D.; Freund, L. B. *Proc. Natl. Acad. Sci. U. S. A.* **2005,** 102, 9469-9474.
19. Jiang, W.; Kim, B. Y. S.; Rutka, J. T.; Chan, W. C. W. *Nat. Nanotechnol.* **2008,** 3, 145-150.
20. Pluen, A.; Netti, P. A.; Jain, R. K.; Berk, D. A. *Biophys. J.* **1999,** 77, 542-52.
21. Chauhan, V. P.; Popovic, Z.; Chen, O.; Cui, J.; Fukumura, D.; Bawendi, M. G.; Jain, R. K. *Angew. Chem., Int. Ed. Engl.* **2011,** 50, 11417-20.
22. Weiss, T. H.; Mills, A. L.; Hornberger, G. M.; Herman, J. S. *Environ. Sci. Technol.* **1995,** 29, 1737-1740.
23. Chithrani, B. D.; Ghazani, A. A.; Chan, W. C. W. *Nano Lett.* **2006,** 6, 662-668.
24. Yang, K.; Ma, Y. Q. *Nat. Nanotechnol.* **2010,** 5, 579-583.
25. Li, L.; Liu, T.; Fu, C.; Tan, L.; Meng, X.; Liu, H. *Nanomedicine* **2015,** 11, 1915-24.
26. Chu, Z.; Zhang, S.; Zhang, B.; Zhang, C.; Fang, C. Y.; Rehor, I.; Cigler, P.; Chang, H. C.; Lin, G.; Liu, R.; Li, Q. *Sci. Rep.* **2014,** 4, 4495.
27. Agarwal, R.; Singh, V.; Jurney, P.; Shi, L.; Sreenivasan, S. V.; Roy, K. *Proc. Natl. Acad. Sci. U. S. A.* **2013,** 110, 17247-52.
28. Geng, Y.; Dalhaimer, P.; Cai, S.; Tsai, R.; Tewari, M.; Minko, T.; Discher, D. E. *Nat. Nanotechnol.* **2007,** 2, 249-55.
29. Barua, S.; Yoo, J. W.; Kolhar, P.; Wakankar, A.; Gokarn, Y. R.; Mitragotri, S. *Proc. Natl. Acad. Sci. U. S. A.* **2013,** 110, 3270-5.
30. Backhed, F.; Ley, R. E.; Sonnenburg, J. L.; Peterson, D. A.; Gordon, J. I. *Science* **2005,** 307, 1915-20.
31. Johansson, M. E.; Sjovall, H.; Hansson, G. C. *Nat. Rev. Gastroenterol. Hepatol.* **2013,** 10, 352-61.
32. Sycuro, L. K.; Pincus, Z.; Gutierrez, K. D.; Biboy, J.; Stern, C. A.; Vollmer, W.; Salama, N. R. *Cell* **2010,** 141, 822-33.
33. Schrank, G. D.; Verwey, W. F. *Infect. Immun.* **1976,** 13, 195-203.
34. Zhang, X.; Li, F.; Guo, S.; Chen, X.; Wang, X.; Li, J.; Gan, Y. *Biomaterials* **2014,** 35, 3650-65.
35. Yu, T.; Malugin, A.; Ghandehari, H. *ACS Nano* **2011,** 5, 5717-28.
36. Huang, X.; Teng, X.; Chen, D.; Tang, F.; He, J. *Biomaterials* **2010,** 31, 438-448.
37. Suh, J.; Dawson, M.; Hanes, J. *Adv. Drug Delivery Rev.* **2005,** 57, 1551-1551.
38. Li, X. Y.; Guo, S. Y.; Zhu, C. L.; Zhu, Q. L.; Gan, Y.; Rantanen, J.; Rahbek, U. L.; Hovgaard, L.; Yang, M. S. *Biomaterials* **2013,** 34, 9678-9687.
39. Plimpton, S. *J. Comput. Phys.* **1995,** 117, 1-19.
40. Ensign, L. M.; Henning, A.; Schneider, C. S.; Maisel, K.; Wang, Y. Y.; Porosoff, M. D.; Cone, R.; Hanes, J. *Mol. Pharmaceutics* **2013,** 10, 2176-82.
41. Decuzzi, P.; Ferrari, M. *Biomaterials* **2006,** 27, 5307-14.

42. Fish, M. B.; Thompson, A. J.; Fromen, C. A.; Eniola-Adefeso, O. *Ind. Eng. Chem. Res.* **2015,** 54, 4043-4059.
43. Champion, J. A.; Katare, Y. K.; Mitragotri, S. *Proc. Natl. Acad. Sci. U. S. A.* **2007,** 104, 11901-4.
44. Euliss, L. E.; DuPont, J. A.; Gratton, S.; DeSimone, J. *Chem. Soc. Rev.* **2006,** 35, 1095-104.

Table of Contents Graphic